Fuel 385 (2025) 134104

Contents lists available at ScienceDirect

Fuel

journal homepage: www.elsevier.com/locate/fuel

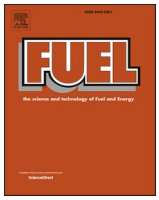

Full Length Article

The investigation of the influence of the addition of cerium dioxide to the anode composition on the internal carbon dioxide conversion of methane on second-generation SOFCs

G.M. Korableva [a], D.A. Agarkov [a,b,*], D.S. Katrich [a], A.V. Samoilov [a], A.U. Sharafutdinov [a], S.I. Bredikhin [a]

[a] Osipyan Institute of Solid State Physics RAS, Academician Osipyan Street, 2, 142432 Chernogolovka, Moscow District, Russia
[b] Moscow Institute of Physics and Technology, Institutsky Lane, 9, 141701 Dolgoprudny, Moscow Region, Russia

ARTICLE INFO

Keywords:
Solid oxide fuel cell
Anode-supported SOFC
Methane internal conversion
Doped ceria
Impregnation
Carbon deposition

ABSTRACT

The effect of the addition of cerium dioxide in different forms – GDC (gadolinia-doped ceria, CeO_2 doped with 10 mol% Gd_2O_3) layer on the surface, CeO_2 nanoparticles – on the results of internal carbon dioxide conversion of methane at the anode of solid oxide fuel cells was studied in the present work. The studies were carried out mainly using a technique that combined electrochemical techniques, Raman spectroscopy, and flow gas analysis. It was shown that the long-term operation of the fuel cell under conditions of carbon dioxide conversion led to the formation of carbon deposits throughout the thickness of the model samples. The presence of carbon was confirmed by the micrographs of a scanning electron microscope, as well as the results of energy-dispersive analysis and Raman spectroscopy. It was found that carbon had a form of graphite inside the fuel electrode. Polymerization of carbon clusters into carbon nanotubes was observed closer to the free surface of the anode. Raman spectroscopy studies showed the presence of D- and G-graphite bands in the spectrum, which also indicated the presence of disordered and filamentary carbon. At the same time, longer exposure to carbon-containing fuel led to an increase in the proportion of carbon polymerized into nanotubes. Cerium dioxide was shown to have a positive effect on the electrochemical characteristics of the cells: the time of stable operation increased, and the amount of carbon deposits decreased even after adding a small amount of CeO_2.

1. Introduction

Solid oxide fuel cells, stacks, and power plants based on them are promising technology for the generation of electrical and high-potential heat energy owing to record high efficiency [1,2]. Currently, modern power plants based on solid oxide fuel cells (SOFCs) often use a mixed type of conversion of the original hydrocarbon fuel when part of the fuel is converted in a device external to the SOFC stack, a fuel processor, and the remaining part (up to 50 %) is converted directly at the SOFC anode [3]. This process is called internal reforming [4,5]. With any type of conversion in the fuel processor (partial oxidation, steam conversion, or autothermal reforming), a certain amount of carbon dioxide (CO_2) is formed [6], which, on average, is a ballast gas and does not participate in further electrochemical reactions. Accordingly, carbon dioxide does not lead to the generation of electrical and thermal energy but requires energy costs for pumping through the power plant systems. On the other hand, in the case of partial internal conversion, the carbon dioxide generated in the fuel processor can be used as a reagent for the carbon dioxide conversion process [7]. This approach is extremely promising [8] in terms of increasing the efficiency of fuel conversion and, ultimately, the overall efficiency of the power plant using this concept.

The mechanisms of carbon dioxide conversion of various hydrocarbons, including methane, have been well studied for the process of conversion in a fuel processor on catalysts standard for this case [9,10]. The process of internal carbon dioxide conversion occurring directly at the SOFC anode using the anode components as catalysts has almost not been studied. For this reason, the mechanisms of internal carbon dioxide conversion of fuel directly at the SOFC anode under fuel chamber conditions were investigated in the present work. Methane was selected as a model fuel for the present studies since natural gas, which mainly

* Corresponding author at: apt. 33, Beregovaya st., 24, 142432 Chernogolovka, Moscow District, Russia.
E-mail addresses: eliseevagm@issp.ac.ru (G.M. Korableva), agarkov@issp.ac.ru (D.A. Agarkov), katrichds@issp.ac.ru (D.S. Katrich), samoilov@issp.ac.ru (A.V. Samoilov), shazat@issp.ac.ru (A.U. Sharafutdinov), bredikh@issp.ac.ru (S.I. Bredikhin).

https://doi.org/10.1016/j.fuel.2024.134104
Received 18 October 2024; Received in revised form 29 November 2024; Accepted 8 December 2024
Available online 17 December 2024

Table 1
Designation, anode, electrolyte, and cathode compositions for the fabricated samples: half-cells and full model anode-supported SOFCs.

Sample designation	Anode	Electrolyte	Cathode
Half-cell			
HC	NiO/YSZ	8YSZ	–
HC GDC	NiO/YSZ GDC layer on the surface	8YSZ	–
HC imp. CeO_2	NiO/YSZ, impregnated CeO_2	8YSZ	–
Model SOFCs			
SOFC	NiO/YSZ	8YSZ + GDC	LSCF
SOFC imp. CeO_2	NiO/YSZ, impregnated CeO_2	8YSZ + GDC	LSCF

consists of it, is a fairly common type of fuel for power plants on solid oxide fuel cells.

2. Methods

Half-cells (supporting anode with applied thin-film electrolyte) and full model anode-supported SOFCs (supporting anode with thin-film electrolyte and cathode) were studied in this work. Table 1 shows the designation and anode, electrolyte, and cathode compositions for the fabricated samples.

In Table 1, YSZ is yttria-stabilized zirconia (ZrO_2 doped with 8 mol% Y_2O_3), GDC is gadolinia-doped ceria (CeO_2 doped with 10 mol% Gd_2O_3), and LSCF is $(La_{0.6}Sr_{0.4})_{0.97}Co_{0.2}Fe_{0.8}O_{3-\delta}$.

Commercially available anode substrates manufactured by Kceracell (Republic of Korea) were used in this work. These are three-layer substrates with a thickness of 700 μm with a ratio of NiO/YSZ ≈ 6/4, onto which a thin-film YSZ electrolyte with a thickness of 6 μm and a barrier layer of GDC with a thickness of about 1 μm were deposited. The layer thicknesses were measured by means of scanning electron microscopy (SEM). These substrates with a size of 100 × 100 mm were cut with a MiniMarker 2-20A4 compact precision marker based on an fiber laser (Russia) on disks with a diameter of 21 mm. Based on these disks, half-cells were manufactured (samples without a cathode and contacts: only as is commercial anode support with thin-film electrolyte and GDC layer):

1. without modifications (*HC* in Table 1),
2. with an additional GDC layer screen-printed on the anode surface (*HC GDC* in Table 1),
3. half-cells impregnated with CeO_2 (*HC imp. CeO_2* in Table 1).

The GDC layer was applied by screen printing using an Ekra E2 machine (Asys Group, Germany). The impregnated particles were prepared using a 2 M aqueous solution of cerium nitrate $Ce(NO_3)_3{\cdot}6H_2O$. The anode surface was wetted with this solution, excess liquid was removed with a napkin, and then the sample was placed in a drying furnace at 250 °C for 1 h to remove water. After drying, the sample was treated using these steps again with a final annealing at 750 °C. The mass of cerium dioxide added to the anode as a result of this procedure was 4–5 % of the mass of the original samples. Impregnation was applied to one type of half-cells (*HC imp. CeO_2* in Table 1) and one type of model SOFCs (*SOFC imp. CeO_2* in Table 1).

In order to fabricate samples for electrochemical testing, commercially available LSCF cathode paste (Kceracell, Republic of Korea) based on powder with a specific surface area of 10–15 m^2/g was applied to half-cells using screen printing on an Ekra E2 machine(Germany); then, the samples were annealed at 1000 °C. This resulted in an LSCF cathode layer with a thickness of ~30 μm. To form contact electrodes gold paste was applied to both sides of the samples in the form of a grid, followed by drying at 100 °C. Gold wires with a diameter of 0.3 mm were attached to the resulting layer using Aron Ceramic E ceramic glue (Japan). Sintering of the contact electrodes occurred during the start-up of the samples at 850 °C. In this case, the use of gold contacts was necessary to ensure current collection and eliminate the effect of platinum on the conversion results since gold is much less catalytically active with respect to methane conversion reactions than platinum or nickel contained in the anode.

Table 2
Outlet gas composition resulting from dry reforming obtained from a half-cell, a half-cell with GDC, and a half-cell impregnated with CeO_2 (all with the supporting anode). The results are given for the inlet fuel mixture with the composition $CH_4/CO_2/N_2$ = 35/35/30 ml/min.

Sample	Composition, vol %				Total flow, ml	The degree of methane conversion, %
	CH_4	CO_2	H_2	CO		
HC	18.7	20.5	12.5	21.9	112	40
HC GDC	22.1	23.8	7.7	19.1	110	31
HC imp. CeO_2	17.6	19.4	14.6	25.9	127	33

The majority of studies were carried out using a technique that combined electrochemical techniques, Raman spectroscopy, and flow gas analysis. This technique was described in detail elsewhere [11–13]. The flow gas analysis of half-cells and model SOFCs during operation was carried out using a Test-1 gas analyzer (Boner LLC, Russia). The electrochemical measurements, mainly those of IV curves and impedance spectra, were carried out using a Reference 3000 potentiostat (Gamry, USA) equipped with an additional Reference 30 K Booster module. The Raman spectroscopy studies were performed using a homemade setup based on a green (532 nm) semiconductor laser, an optical system for the collection of scattered radiation, and a nitrogen-cooled CCD matrix (Princeton Instruments, USA) to collect the final spectra.

The optical images were collected using an Olympus BX51 optical microscope (Japan).

The thermodynamic calculations were performed in HSC Chemistry 9. The ternary phase diagram C-O-H_2 was calculated using the Wolfram Mathematica software.

The microstructure of the samples was studied by means of SEM using Supra 50 VP (Oxford Diffraction) equipped with an INCA + microanalysis system.

3. Results and discussion

In this work, at first studies of half-cells with various modifications of the anode (3 types of half-cells listed in section 2 Methods) were carried out, namely influence of these modifications on the results of methane conversion and degradation rate was estimated. The next step of our research was to manufacture model SOFC samples with same modifications to study electrochemical characteristics and effect of current load on methane conversion conditions.

3.1. Studies of half-cells

In the first part of the study, half-cells with different compositions were investigated during the internal dry (by carbon dioxide) reforming of methane (IDRM) at 750 ℃. The experiment was carried out according to the following scheme. First, the sample was kept in an inert atmosphere. Then, the cermet anode was reduced in a dry hydrogen–nitrogen mixture with an H_2 content of up to 50 %. Preliminary reduction of the fuel electrode was necessary to form a sufficient amount of nickel in the material since it is a catalyst for methane conversion. Then, to clean the fuel chamber from hydrogen, a switch to an inert atmosphere occurred. After that, a fuel mixture with a given composition $CH_4/CO_2/N_2$ = 35/35/30 ml/min was fed into the anode chamber.

Table 2 presents the results of the compositions of the outlet mixtures in the IDRM process for all half-cell samples 30 min after the start of conversion. The impregnated half-cell (highlighted in Table 2) has the

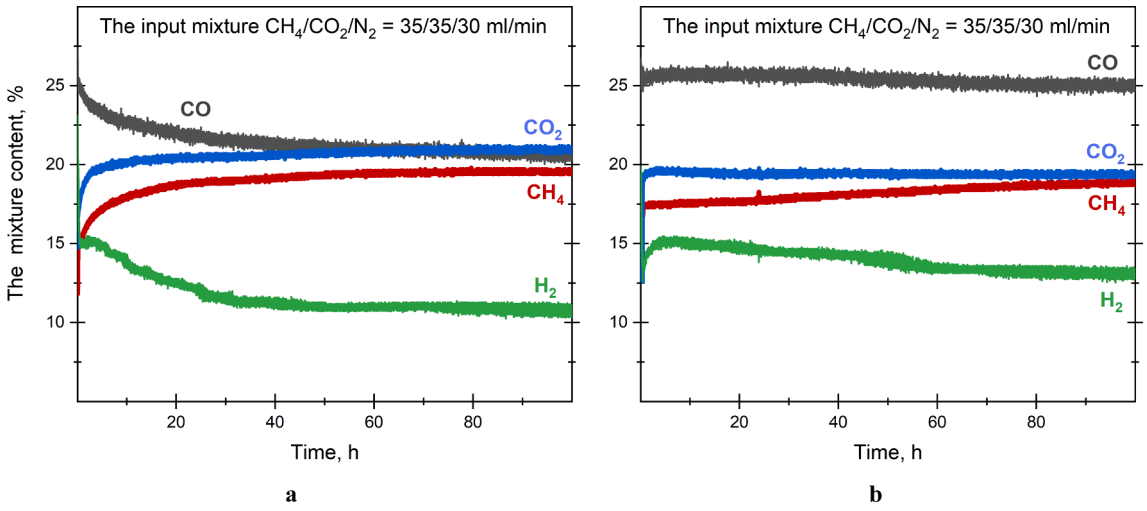

Fig. 1. **a** – Time dependence of the outlet gas composition when feeding the fuel mixture $CH_4/CO_2/N_2 = 35/35/30$ ml/min into the initial half-cell *(HC)*, **b** – half-cell impregnated with CeO_2 (*HC imp. CeO₂*) for a long time at 750 °C.

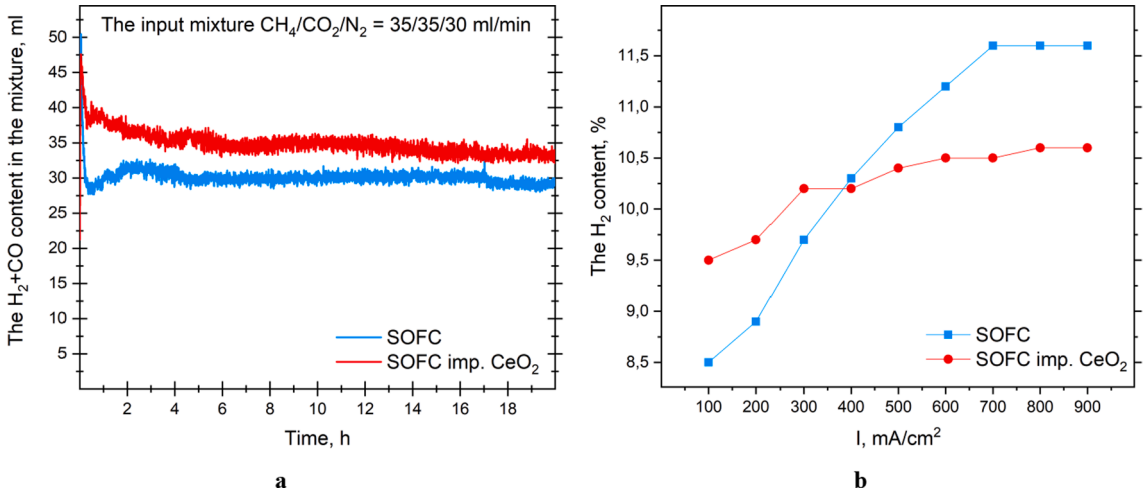

Fig. 2. **a** – Comparison of the synthesis gas content in the outlet gas mixtures obtained from model SOFCs with the anode-supported structure at 750 °C, **b** – the effect of the current load on the hydrogen content in the output mixture.

highest values of flow, hydrogen and carbon monoxide content in the outlet mixture.

The results show that the sample with a GDC layer has the lowest characteristics. This is most likely due to the fact that the resulting layer (3 μm) was too dense and prevented the free diffusion of reagents into the electrode. Due to the unsatisfactory results of the half-cells with GDC, further studies of model SOFCs with such anode composition were not carried out.

Fig. 1 illustrates the results of the life tests (over 100 h) in the process of IDRM on half-cells.

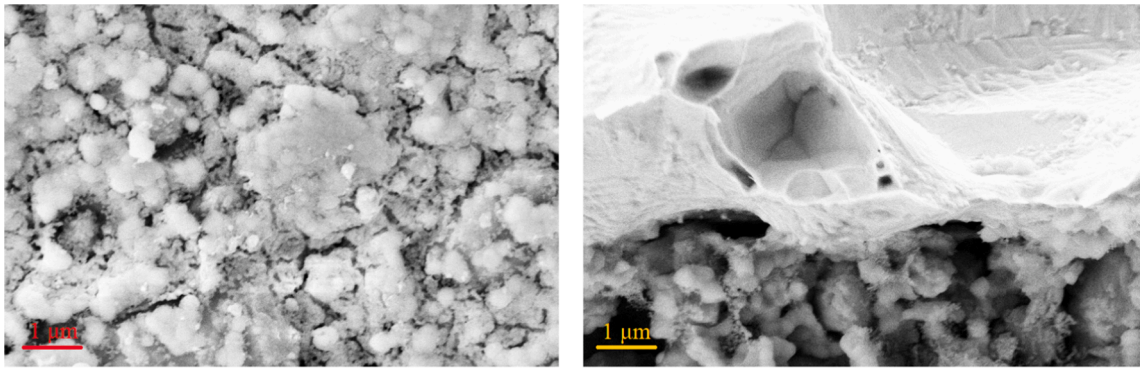

Fig. 3. Micrographs of the surface (**a**) and the near-surface layer of the cross-section (**b**) of the model SOFC's anode with CeO_2 impregnation.

Table 3
Comparison of the outlet gas composition obtained from a model *SOFC* and a SOFC impregnated with CeO_2 (*SOFC imp. CeO_2*) during dry reforming of methane. The results are given for the inlet fuel mixture with the composition $CH_4/CO_2/N_2 = 35/35/30$ ml/min.

Sample	Composition, vol %				Total flow, ml	The degree of methane conversion, %
	CH_4	CO_2	H_2	CO		
OCV conditions						
SOFC	22.4	25.4	8.2	17.5	113	28
SOFC imp. CeO_2	21.5	23.1	8.9	19.9	119	31
Under current load of 500 mA/cm^2						
SOFC	19.6	24.5	10.9	19.5	117	34
SOFC imp. CeO_2	19.5	23.6	10.8	19.8	114	36

During the first day, hydrogen content in the sample without modifications decreased by more than 20 %. This decrease is due to the deposition of carbon onto the active areas of the anode which as a result are separated from the gas phase and cease to participate in the conversion processes. By the active areas here we mean surface of nickel particles, especially the triple-phase boundary that occurs when interface between nickel and YSZ particles meets the gas environment (gas phase). In the case of the sample impregnated with cerium dioxide, a decrease in the proportion of hydrogen over the entire period of life tests was less than 10 %. This is due to the fact that cerium dioxide introduced into the anode prevents the formation of carbon deposits, which leads to the maintenance of catalytic activity at a high level for a long time.

3.2. Studies of model SOFCs

As mentioned above, only two types of model SOFCs were manufactured based on data obtained during half-cells studies. Namely, SOFCs without modifications and samples with anode impregnated by CeO_2 (similar procedure resulting in 4–5 wt% addition).

Fig. 2a depicts the comparison of the synthesis gas ($H_2 + CO$) content in the outlet gas mixtures obtained from model SOFCs with the anode-supported structure at 750 °C.

Firstly, the analysis of gases in the outlet mixture for model SOFC samples studied (Fig. 2a) shows that the sample with impregnated anode have a higher yield of synthesis gas compared to similar unmodified sample. This corresponds to the data obtained from half-cell samples and indicates the positive effect of CeO_2 addition on results of conversion.

The electrochemical tests (Fig. 2b) show that at low current load values, the hydrogen content in the outlet mixture is slightly higher for the sample impregnated with cerium dioxide. However, starting from 400-500 mA/cm^2, the hydrogen content almost stops growing and becomes lower than in the case of the sample without modifications. This can be related to the partial blockage of the pores at the anode with agglomerates of cerium dioxide particles that hinder the diffusion of reagents in the anode. Subsequent SEM images (Fig. 3) also support that hypothesis as one can see areas of dense CeO_2 clusters on the surface of anode.

It is worth noting that at current densities of more than 700 mA/cm^2, the sample without impregnation reaches a “plateau” in the hydrogen content, which is most likely due to the maximum degree of methane conversion under experimental conditions.

Table 3 summarizes the results of the gas analysis for the model SOFC samples under open-circuit voltage (OCV) conditions and at a current load of 500 mA/cm^2.

As noted earlier, under open-circuit conditions, the sample impregnated with cerium dioxide demonstrates a higher degree of methane conversion (and a higher total flow due to the increased amount of outlet synthesis gas) compared to the sample without impregnation. However, when applying a current load of about 500 mA/cm^2, the percentage of reactants in the mixture is almost equal for both samples, although the degree of methane conversion remains higher in the case of the sample with cerium dioxide.

Fig. 4a shows the IV and power curves of two types of SOFCs for different fuel mixture compositions: $H_2/N_2 = 50/50$ ml/min and $CH_4/CO_2/N_2 = 35/35/30$ ml/min.

When feeding a hydrogen–nitrogen mixture, the open-circuit voltage for the SOFCs with and without modifications is more than 1.03 V, indicating a high quality of cell sealing and the absence of gas or electron leaks, which, in turn, makes it possible to perform accurate electrochemical measurements. When studying the IV and power curves of model SOFC samples (Fig. 4a), a positive effect of the cerium dioxide additive was also revealed, namely, an increase in the maximum power density by about 10 % in both the hydrogen–nitrogen and IDRM mixtures. It is worth noting a decrease in the power density when switching from a hydrogen-containing mixture to an IDRM mixture. It is caused by an increase in the polarization resistance of the samples (Fig. 4b) when changing the fuel mixture.

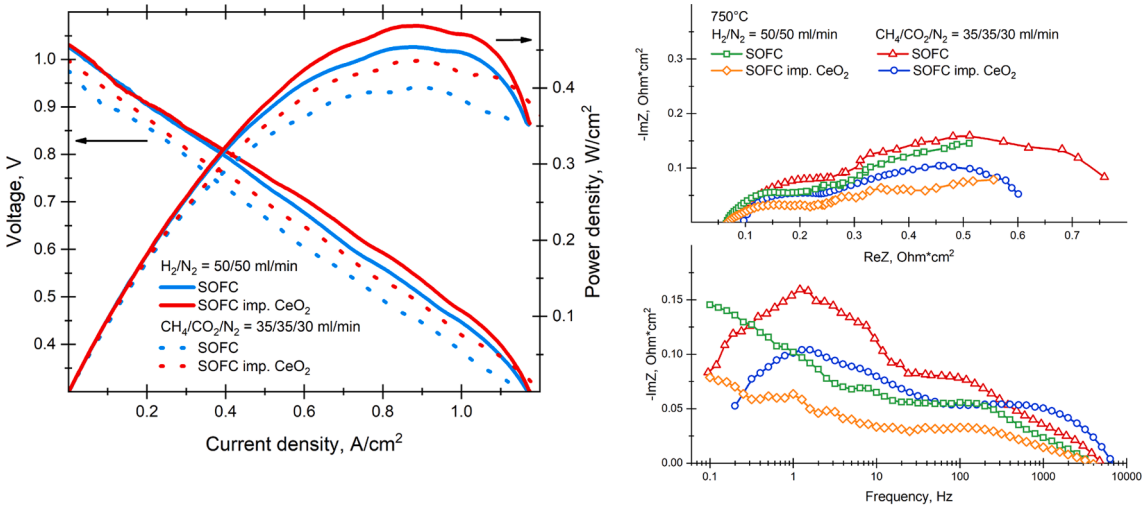

Fig. 4. **a** – IV and power curves, **b** – impedance spectra of model SOFCs under OCV conditions in fuel mixtures of $H_2/N_2 = 50/50$ ml/min and $CH_4/CO_2/N_2 = 35/35/30$ ml/min at a 750 °C.

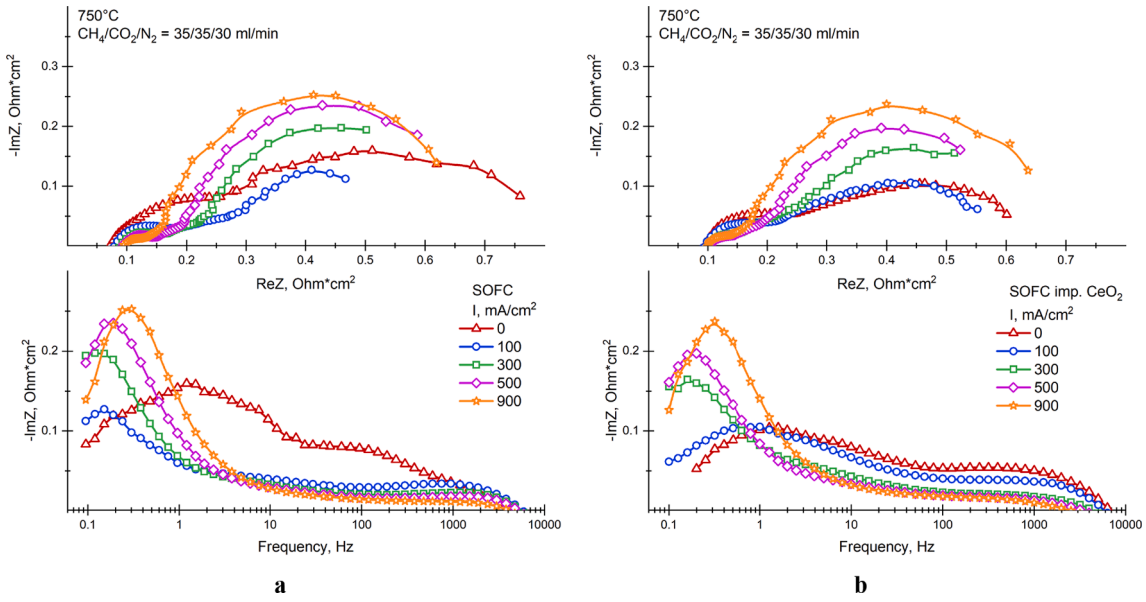

Fig. 5. Effect of current load on the impedance spectra obtained from model SOFCs under IDRM conditions: **a** – model SOFC without modifications (*SOFC*), **b** – model SOFC impregnated with cerium dioxide (*SOFC imp. CeO_2*).

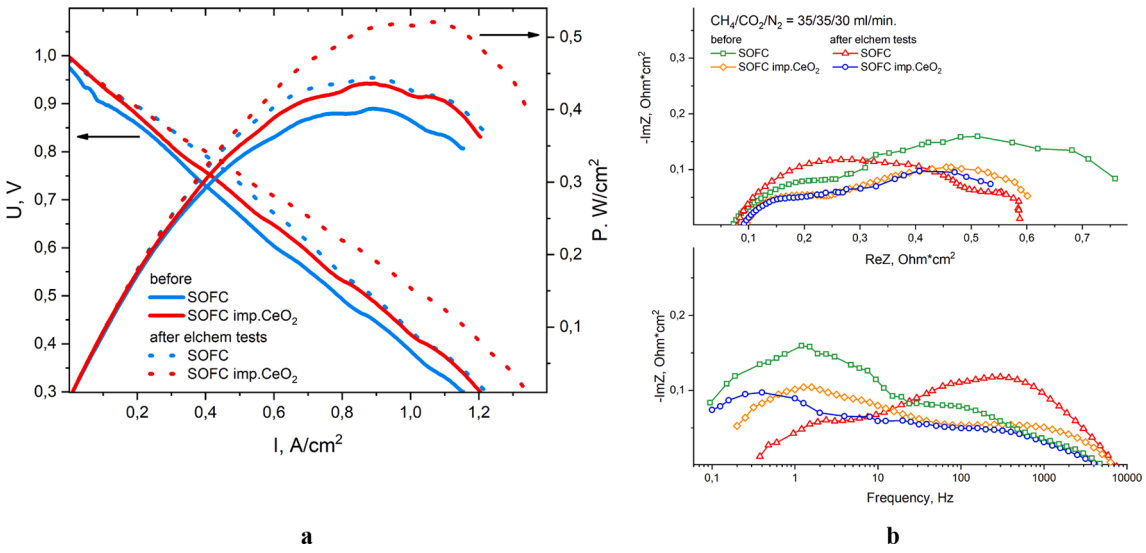

Fig. 6. **a** – IV and power curves and **b** – impedance spectra of model SOFCs at the beginning of the experiment (before) and after electrochemical tests in fuel mixture $CH_4/CO_2/N_2$ = 35/35/30 ml/min at a 750 °C.

Fig. 5 depicts the impedance spectra of model SOFCs with different compositions under current load conditions.

The impedance spectra at different current loads indicate a decrease in the high- and middle-frequency contributions to the polarization resistance, which correspond to activation processes and processes associated with the kinetics of reactions, respectively. This change is caused by local heating of the fuel cell due to Joule heating. In the low-frequency region associated with diffusion processes, a gradual increase in the contribution is observed as the current density increases, which is due to an increase in the amount of fuel/oxidizer required for oxidation reactions to occur.

All electrochemical tests mentioned above (initial measurements of IV curves and impedance spectroscopy as well as subsequent measurements under different current loads) were then followed by similar final measurements to investigate the performance degradation. Fig. 6 shows the comparison of the impedance spectra, IV and power curves of model SOFCs before and after electrochemical tests.

Comparison of the current–voltage characteristics (Fig. 6a) before and after electrochemical tests under IDRM conditions shows that for both model SOFC the resistance decreases (as can be seen from the decrease in the slope of the IV curve). For the sample without modifications, a strong change in the impedance spectrum is observed (Fig. 6b). A sharp decrease in the low-frequency and an increase in the mid-frequency contributions to the impedance indicate that the processes of gas diffusion into the anode have been facilitated compared to the initial stage of the studies, while the reaction kinetics have slowed down significantly. A possible explanation for this is the irreversible degradation of the anode caused by partial destruction of its surface layer (the pores expand, but the area of the TPB decreases). However, this was not detected in SEM studies. In turn, the impedance analysis (Fig. 6b) for the model SOFC impregnated with ceria indicates an insignificant decrease in the low-frequency contribution to the impedance. This can be caused by current load: on the one hand, due to the effect on the resistance of the cathode [14], on the other hand, due to the

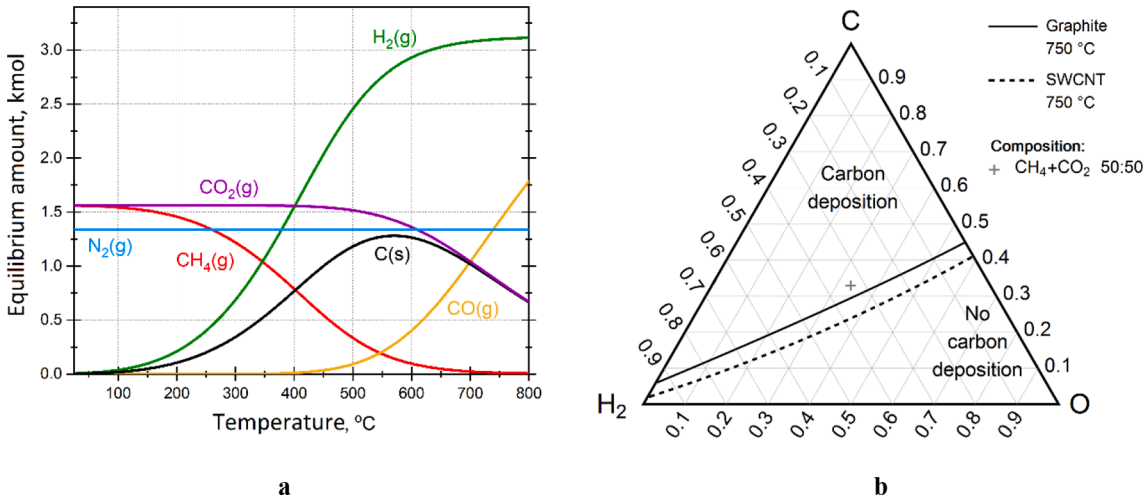

Fig. 7. a – thermodynamic calculations of the process of dry reforming of methane depending on temperature, b – ternary phase diagram c-o-h_2, the cross marks the composition of the fuel mixture for carbon dioxide conversion of methane. The solid line is the boundary of graphite deposition, and the dashed line "SWCNT" is the boundary of single-wall carbon nanotube deposition [17,18].

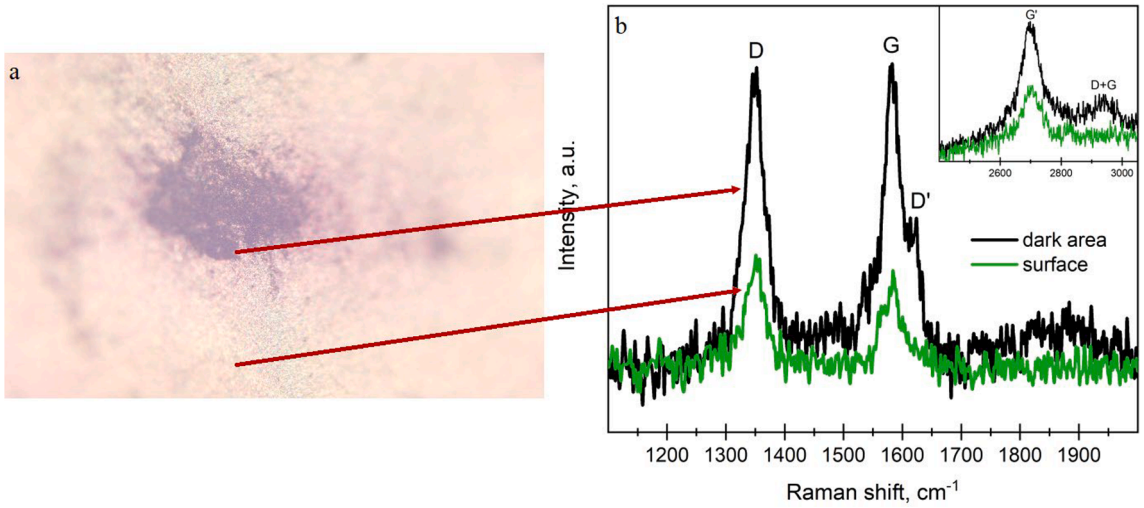

Fig. 8. **a** – Photograph of the surface of the anode-supported half-cell after operation in the carbon-containing fuel obtained using an optical microscope. **b** – Raman spectra obtained ex situ from a clean surface and a dark area on the half-cell surface. The inset is a distant region of wave numbers.

removal of carbon deposits from the anode [15,16].

Fig. 7 shows the thermodynamic calculations of the process of dry reforming of methane depending on temperature.

The thermodynamic calculations of the carbon dioxide conversion of methane (Fig. 7a) show that at the temperature of interest (750 °C), almost complete conversion of methane occurs, while about half of the carbon monoxide formed is again combined into CO_2 molecules as a result of the Boudoir reaction, which is accompanied by carbon deposition. From additional thermodynamic calculations under experimental conditions (Fig. 7b), we can draw a conclusion about the form of carbon deposits formed at the anodes during the conversion. However, these calculations do not take into account the kinetics of the processes; therefore, the formation of both forms of carbon is quite likely under experimental conditions. The presence of nitrogen in the mixture leads to a slight shift in the deposition boundaries of both graphite and nanotubes. Based on these data, this particular mixture ($CH_4/CO_2/N_2$ = 35/35/30 ml/min) was selected for conducting the experiments since the system is then for sure in the carbon deposition region, which allows one to study the conversion processes, as well as to conduct research of both the carbon deposits themselves and the effect of anode modifications on the intensity of their deposition.

Table 4
Frequencies, half-widths, and intensity ratios of carbon lines for different samples.

Sample	Line, cm^{-1}			Half-width, cm^{-1}		Intensity ratio
	D	G	D'	ΔD	ΔG	$R = I_D/I_G$
SOFC	1350	1583	1619	50.5	29.5	0.693
HC dark area	1349	1582	1621	40.3	35.9	0.971
HC "clean" area	1351	1584	–	39.1	28.2	1.127

After long-term tests of the samples in the dry reforming mode, the formation of various dark spots and stripes was observed on the surface of the samples. Fig. 6a depicts a photograph of the surface of the sample under study with a dark area.

The Raman spectra obtained from this dark region on the sample surface (Fig. 8b) revealed several lines related to carbon. Thus, the lines G (1580 cm^{-1}) and G′ (2670 cm^{-1}) correspond to a highly ordered form of graphite, and the emergence of the lines D (1350 cm^{-1}) and D′ (1610 cm^{-1}) is due to the presence of defect structures, such as soot or defective ends of carbon nanotubes. Moreover, the peak D + G (2900

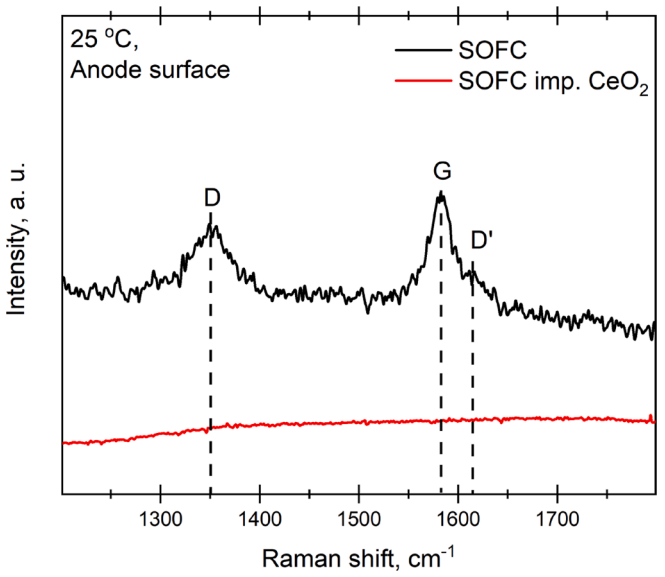

Fig. 9. Comparison of the Raman spectra obtained ex situ from the surface of the model SOFC sample without modification (*SOFC*) and that with impregnation with cerium dioxide (*SOFC imp. CeO_2*) after long-term tests in the carbon-containing fuel.

cm^{-1}) arises as a result of double resonance scattering on the defects.

Table 4 shows the calculations of the positions of the lines D, G, and D', their half-widths, and the intensity ratio $R = I_D/I_G$. These values were obtained using the approximation of the Lorentz function.

Fig. 9 depicts the comparison of the Raman spectra of the surfaces of the model SOFC samples after the IDRM process. It is evident that the amount of carbon deposits at the anode of the impregnated sample is reduced to such an extent that they cannot be detected by Raman spectroscopy. Subsequent SEM studies confirm the presence of various forms of carbon at the anode of the model SOFC without CeO_2 impregnation, as well as a significant reduction in the amount of carbon deposits on the samples with added cerium dioxide.

In the micrograph of the cross-section of the half-cell without impregnation (*HC*) before the experiments (Fig. 10a), there are relatively large particles of nickel oxide which are surrounded by smaller particles of stabilized zirconium dioxide. When comparing the cross-sectional images of the samples before and after the tests (Fig. 10a and 10b, respectively), structural changes in the anode can be seen: the size of the nickel grains decreases and their morphology changes. These changes are also accompanied by carbon deposition on the surface of the nickel grains, which will be discussed below.

Table 5
Results of the energy-dispersive analysis of the surface of the half-cell and model SOFC after operation in the carbon-containing fuel.

Sample	Weight, %					
	C	O	Ni	Zr	Ce	Gd
HC – "clean" area	21.26	13.47	27.21	27.34	–	–
HC – dark area	31.99	14.53	33.11	31.10	–	–
HC with GDC	1.24	17.7	0.28	–	72.18	8.59
SOFC imp. CeO_2	1.93	19.26	35.59	34.60	8.62	–

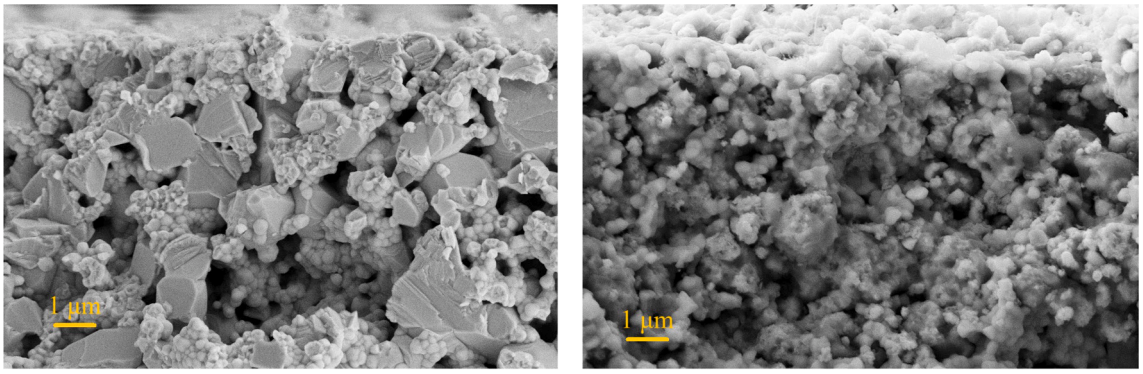

a **b**

Fig. 10. Micrographs of the near-surface layer of the cross-section of the fuel electrode before testing (**a**) and after long-term operation in the carbon-containing fuel at 750 ℃ (**b**).

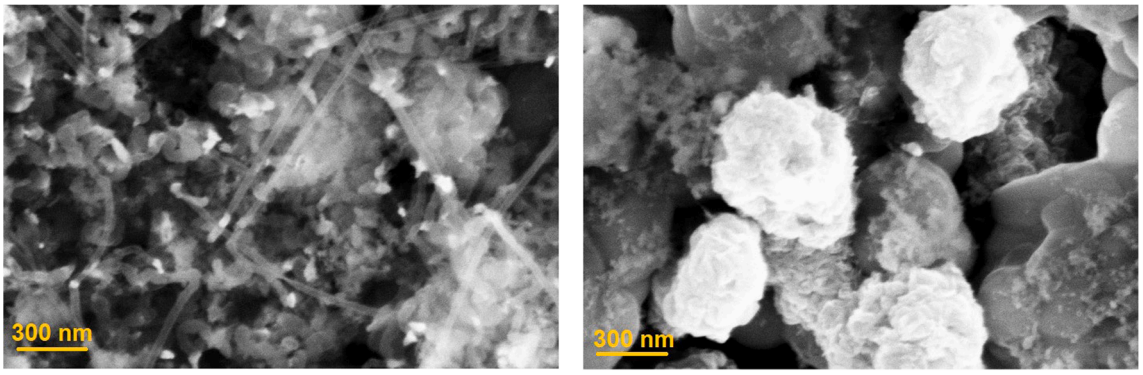

a **b**

Fig. 11. Micrographs of the fuel electrode surface of the half-cell (**a**) and the model SOFC (**b**) after long-term operation in the carbon-containing fuel at 750 ℃.

Fig. 11a shows a micrograph of the area that was visually darker during the initial inspection of the sample after the testing. One can see carbon sediments present on the surface of the sample. Considering the data obtained from Raman spectroscopy studies we assume that these oblong structures are carbon nanotubes. It is to be noted that there is no noticeable growth of them into the electrode. A micrograph of the surface of the model SOFC after similar tests (Fig. 11b) also indicates structural changes in the anode and carbon deposition, but carbon nanotubes are no longer observed.

The results of the energy-dispersive analysis (Table 5) of the sample surface after carbon dioxide conversion also indicate a significant decrease in the amount of deposited carbon on the samples containing cerium dioxide. From these data, it is evident that the sample with the GDC layer containing the largest amount of CeO_2 has the smallest amount of carbon deposits on its surface. However, the result for the impregnated sample shows that a much smaller amount of cerium dioxide is sufficient to effectively prevent carbon deposition on the surface of nickel particles.

4. Conclusions

The internal carbon dioxide conversion of methane in an anode-supported SOFC was investigated in the present work by means of a combined setup using electrochemical techniques, Raman spectroscopy, and flow gas analysis. The studies began with half-cells: samples of anode support with applied electrolyte but without cathode and contacts. The results of the analysis of the outlet gas mixture in the process of carbon dioxide conversion of methane on these samples with various modifications revealed that impregnation of the anode with cerium dioxide leads, on the one hand, to an increase in hydrogen and carbon monoxide content, and on the other hand, to a decrease in the degradation rate. Model SOFCs for electrochemical testing were manufactured based on data obtained during half-cells studies. Analysis of outlet mixtures in similar tests for these model SOFC also confirms the findings of the previous stage.

The results of the electrochemical studies showed that the replacement of the hydrogen–nitrogen fuel mixture with the carbon-containing one led to a noticeable deterioration in the characteristics of the anode-supported solid oxide fuel cell. The overall resistance of the sample increased mainly due to an increase in the middle-frequency contribution to the polarization resistance associated with an increase in the time of the reaction kinetics. It was also shown that the long-term operation of a solid oxide fuel cell under IDRM conditions resulted in the formation of carbon deposits throughout the thickness of the model samples. The presence of a significant amount of carbon (up to 40 wt%) was confirmed by the micrographs of the scanning electron microscope and the results of the energy-dispersive analysis and Raman spectroscopy. It was established that inside the fuel electrode, carbon was in the form of graphite; when approaching the free surface, polymerization of carbon clusters into carbon nanotubes was observed. The study of the fuel cell surface using Raman spectroscopy showed the presence of D- and G-bands, which indicated the presence of both disordered and filamentary carbon. At the same time, longer exposure to the carbon-containing fuel led to an increase in the proportion of carbon polymerized into nanotubes. Moreover, the addition of cerium dioxide nanoparticles to the anode composition by impregnation led to a noticeable suppression of carbon deposition on the surface of the cermet anode, which made it possible to increase the amount of synthesis gas produced, slightly improve the electrochemical characteristics, and increase the duration of stable operation in the IDRM mode.

Therefore, cerium dioxide had a positive effect on the electrochemical characteristics of the cells: the time of stable operation increased (rate of degradation decreased), and the amount of carbon deposits decreased even after adding a small amount of cerium dioxide.

CRediT authorship contribution statement

G.M. Korableva: Writing – original draft, Investigation, Data curation. **D.A. Agarkov:** Writing – review & editing, Conceptualization. **D.S. Katrich:** Investigation, Data curation. **A.V. Samoilov:** Methodology, Conceptualization. **A.U. Sharafutdinov:** Investigation. **S.I. Bredikhin:** Supervision, Conceptualization.

Declaration of competing interest

The authors declare that they have no known competing financial interests or personal relationships that could have appeared to influence the work reported in this paper.

Acknowledgments

This work was financially supported by the Russian Science Foundation (RSF), grant No. 24-79-10211. Authors also acknowledge support of the Research Facility Center at the ISSP RAS in the part of scanning microscopy studies.

References

[1] Singh M, Zappa D, Comini E. Solid oxide fuel cell: Decade of progress, future perspectives and challenges. Int J Hydrog Energy 2021;46(54):27643–74. https://doi.org/10.1016/j.ijhydene.2021.06.020.
[2] Hussain S, Yangping L. Review of solid oxide fuel cell materials: cathode, anode, and electrolyte. Energy Transit 2020;4(2):113–26. https://doi.org/10.1007/s41825-020-00029-8.
[3] Kupecki J, Motylinski K, Milewski J. Dynamic analysis of direct internal reforming in a SOFC stack with electrolyte-supported cells using a quasi-1D model. Appl Energy 2018;227:198–205. https://doi.org/10.1016/j.apenergy.2017.07.122.
[4] Samoilov AV, Agarkov DA, Fedotov YS, Bredikhin SI. Internal conversion in the membrane-supported SOFC. ECS Trans 2021;103(1):211–9. https://doi.org/10.1149/10301.0211ecst.
[5] Janardhanan VM, Heuveline V, Deutschmann O. Performance analysis of a SOFC under direct internal reforming conditions. J Power Sources 2007;172(1):296–307. https://doi.org/10.1016/j.jpowsour.2007.07.008.
[6] Lee DK, Baek IH, Yoon WL. Modeling and simulation for the methane steam reforming enhanced by in situ CO2 removal utilizing the CaO carbonation for H2 production. Chem Eng Sci 2004;59(4):931–42. https://doi.org/10.1016/j.ces.2003.12.011.
[7] Li Z, Lin Q, Li M, et al. Recent advances in process and catalyst for CO2 reforming of methane. 110312 Renew Sust Energ Rev 2020;134. https://doi.org/10.1016/j.rser.2020.110312.
[8] Nedolivko VV, Zasypalov GO, Vutolkina AV, et al. Carbon dioxide reforming of methane. Russ J Appl Chem 2020;93(6):765–87. https://doi.org/10.1134/S1070427220060014.
[9] Owgi AHK, Jalil AA, Hussain I, et al. Catalytic systems for enhanced carbon dioxide reforming of methane: a review. Environ Chem Lett 2021;19(3):2157–83. https://doi.org/10.1007/s10311-020-01164-w.
[10] Farooqi AS, Yusuf M, Mohd Zabidi NA, et al. A comprehensive review on improving the production of rich-hydrogen via combined steam and CO2 reforming of methane over Ni-based catalysts. Int J Hydrog Energy 2021;46(60):31024–40. https://doi.org/10.1016/j.ijhydene.2021.01.049.
[11] Korableva GM, Agarkov DA, Burmistrov IN, et al. Application of high-temperature Raman spectroscopy (RS) for studies of electrochemical processes in solid oxide fuel cells (SOFCs) and functional properties of their components. ECS Trans 2021;103(1):1301–17. https://doi.org/10.1149/10301.1301ecst.
[12] Eliseeva GM, Burmistrov IN, Agarkov DA, et al. In-situ Raman spectroscopy studies of oxygen spillover at solid oxide fuel cell anodes. Chem Prob 2020;18(1):9–19. https://doi.org/10.32737/2221-8688-2020-1-9-19.
[13] Agarkov DA, Burmistrov IN, Tsybrov FM, Tartakovskii II, Kharton VV, Bredikhin SI. In-situ Raman spectroscopy analysis of the interfaces between Ni-based SOFC anodes and stabilized zirconia electrolyte. Solid State Ion 2017;302:133–7. https://doi.org/10.1016/j.ssi.2016.12.034.
[14] Haanappel VAC, Mai A, Mertens J. Electrode activation of anode-supported SOFCs with LSM- or LSCF-type cathodes. Solid State Ion 2006;177(19–25):2033–7. https://doi.org/10.1016/j.ssi.2005.12.038.
[15] Klein JM, Hénault M, Roux C, Bultel Y, Georges S. Direct methane solid oxide fuel cell working by gradual internal steam reforming: analysis of operation. J Power Sources 2009;193(1):331–7. https://doi.org/10.1016/j.jpowsour.2008.11.122.

[16] Weber A, Sauer B, Müller AC, Herbstritt D, Ivers-Tiffée E. Oxidation of H2, CO and methane in SOFCs with Ni/YSZ-cermet anodes. Solid State Ion 2002;152–153: 543–50. https://doi.org/10.1016/S0167-2738(02)00359-4.
[17] Jaworski Z, Zakrzewska B, Pianko-Oprych P. On thermodynamic equilibrium of carbon deposition from gaseous C-H-O mixtures: updating for nanotubes. Rev Chem Eng 2017;33(3):217–35. https://doi.org/10.1515/revce-2016-0022.
[18] Ribeiro TR, Ferreira Neto JB, Takano C, Poço JGR, Kolbeinsen L, Ringdalen E. C–O–H2 ternary diagram for evaluation of carbon activity in CH4-containing gas mixtures. J Mater Res Technol 2021;13:1576–85. https://doi.org/10.1016/j.jmrt.2021.05.033.